Eur. Phys. J. C 13, 175–184 (2000)
Digital Object Identifier (DOI) 10.1007/s100520000249

THE EUROPEAN PHYSICAL JOURNAL C


# Pair production of charged MSSM Higgs bosons by gluon fusion

O. Brein[a], W. Hollik[b]

Institut für Theoretische Physik, Universität Karlsruhe, 76128 Karlsruhe, Germany

Received: 20 September 1999 / Published online: 27 January 2000 – © Springer-Verlag 2000

**Abstract.** The production of pairs of charged Higgs bosons as predicted by the minimal supersymmetric standard model (MSSM) via the gluon fusion mechanism is investigated. The amplitudes at the leading one-loop order for the parton process $gg \to H^+H^-$ are calculated with the complete set of MSSM particles. Numerical results are presented for the cross section of the inclusive hadron process $pp \to gg \to H^+H^- + X$ at the LHC.

## 1 Introduction

The search for Higgs bosons and the study of the mechanism for the electroweak symmetry breaking is a basic task for future high energy colliders. Charged Higgs particles are part of an extended scalar sector with at least two isodoublets of Higgs fields. Such a minimal scenario with two Higgs doublets is realized in the minimal supersymmetric standard model (MSSM). A possible detection of charged Higgs particles would therefore be a clear signal for the presence of non-standard physics, with a strong hint towards supersymmetry. For an accurate identification a precise determination of the production and decay properties of the non-standard particles is a crucial requirement. At hadron colliders, $H^+H^-$ pairs can be produced by two basic mechanisms: annihilation of quark-antiquark pairs and gluon-gluon fusion. The gluon fusion mechanism is particularly interesting since, as a loop-induced higher-order process, it depends on all virtual particles with couplings to gluons as well as to Higgs bosons. In the MSSM, at the one-loop level, the process is mediated through quarks and squarks (predominantly from the third generation), involving also neutral Higgs bosons and the Higgs self-interaction. Although the cross section for $H^+H^-$ production by $q\bar{q}$ annihilation [1,2] is larger, it is less sensitive to the details of the underlying model than the gluon fusion mechanism. In particular, through the virtual presence of scalar quarks, the MSSM cross section in general is different from the cross section for a non-supersymmetric two-doublet-model even with identical Yukawa couplings. At the LHC, the supression of the cross section for $gg \to H^+H^-$ by a factor $\alpha_S^2$ compared to $q\bar{q} \to H^+H^-$ is partly compensated by the high gluon luminosity.

Gluon fusion into charged Higgs particles has been studied previously in [3] based on the loop contributions from top and bottom quarks. Scalar quark contributions are neglected, which corresponds to the decoupling scenario of sufficiently heavy squarks. In this article we extend the calculation by including also a non-decoupling scalar quark sector in the loop diagrams; we give analytical results and a detailed discussion for the size of the various contributions. In a quite recent paper [4] the squark loops to the gluon fusion process have also been derived. We find agreement with our results.

The paper is organized as follows: After a short description of the MSSM entries for the calculation of the $H^+H^-$ cross section, we derive the parton cross section in Sect. 3. Section 4 contains the hadronic cross section and a numerical analysis. The appendix collects the analytical expressions, the list of coupling constants, and the Feynman graphs for the gluon fusion process.

## 2 MSSM entries

The cross section for $H^+H^-$ production by the lowest order Drell-Yan mechanism depends only on the mass $m_{H^\pm}$ and the gauge couplings of the charged Higgs boson. $H^+H^-$ pair production via gluon fusion, as a higher-order process merging the strong and electroweak interactions, depends on the detailed structure of the Higgs and the quark/squark sector of the MSSM.

### 2.1 Higgs sector

Besides the charged Higgs particles $H^\pm$, the MSSM Higgs sector contains the two neutral CP-even scalars[1] $H_1^0, H_2^0$ and the neutral CP-odd 'pseudoscalar' $A^0$ as physical mass eigenstates. The free parameters of the Higgs sector are frequently chosen to be the mass $m_A$ of the $A^0$ boson and

[a] e-mail: obr@itp.uni-karlsruhe.de
[b] e-mail: Wolfgang.Hollik@physik.uni-karlsruhe.de

[1] The notation $H_1^0$, $H_2^0$ is equivalent to $H^0$, $h^0$ in the conventions of [7]

$$M^2_{\tilde{\mathrm{t}}} = \begin{pmatrix} M^2_{\tilde{Q}} + m_t^2 + m_Z^2(\frac{1}{2} - e_t s_w^2)\cos 2\beta & m_t(A_t - \mu\cot\beta) \\ m_t(A_t - \mu\cot\beta) & M^2_{\tilde{U}} + m_t^2 + m_Z^2 e_t s_w^2 \cos 2\beta \end{pmatrix} \quad , \tag{4}$$

$$M^2_{\tilde{\mathrm{b}}} = \begin{pmatrix} M^2_{\tilde{Q}} + m_b^2 + m_Z^2(-\frac{1}{2} - e_b s_w^2)\cos 2\beta & m_b(A_b - \mu\tan\beta) \\ m_b(A_b - \mu\tan\beta) & M^2_{\tilde{D}} + m_b^2 + m_Z^2 e_b s_w^2 \cos 2\beta \end{pmatrix} \quad , \tag{5}$$

the ratio $\tan\beta = v_2/v_1$ of the vacuum expectation values of the two Higgs doublets. For the present analysis it is more convenient to choose the mass $m_{H^\pm}$ of the charged particles instead of $m_A$ as the free mass parameter. The relation between $m_{H^\pm}$ and $m_A$ in lowest order is given by

$$m^2_{H^\pm} = m_W^2 + m_A^2 \tag{1}$$

with the $W$ mass $m_W$. The CP-even Higgs masses, at the tree level, are given by:

$$m^2_{H^0_1,H^0_2} = \frac{1}{2}\Big[m_A^2 + m_Z^2 \pm\sqrt{(m_A^2+m_Z^2)^2 - 4m_Z^2 m_A^2\cos^2 2\beta}\Big] \quad . \tag{2}$$

The angle $\alpha$ of the rotation diagonalizing the neutral CP-even mass matrix, an entry in several coupling constants, fulfills the tree level relation

$$\tan 2\alpha = \frac{m_H^2 + m_h^2}{m_A^2 - m_Z^2}\tan 2\beta \quad . \tag{3}$$

Both relations (2) and (3) are sizeably modified by quantum corrections, predominantly proportional to $m_t^4$. They are taken into account in the approximation given in [5]. The relation (1) between $m_A$ and $m_{H^\pm}$ is also modified by radiative corrections [6]; the effects, however, are essentially smaller and are neglected in our analysis.

### 2.2 Squark sector

The main entries from the scalar quark sector are from the third generation of top $(\tilde{\mathrm{t}}_L, \tilde{\mathrm{t}}_R)$ and bottom $(\tilde{\mathrm{b}}_L, \tilde{\mathrm{b}}_R)$ squarks. For simplicity we assume a flavor-diagonal squark sector. For the $\tilde{\mathrm{t}}$ and $\tilde{\mathrm{b}}$ case the mass matrices have the form see (4) and (5) on top of the page, and analogously for the other generations. The symbols $e_t$ and $e_b$ denote the electric charge of top- and bottom-quarks; $\mu$ is the supersymmetric Higgs mass parameter[2], $M_{\tilde{Q}}$ the soft-breaking mass parameter for the squark isodoublet $(\tilde{\mathrm{t}}_L, \tilde{\mathrm{b}}_L)$, and $M_{\tilde{U}}$ and $M_{\tilde{D}}$ are the soft-breaking mass parameters for the isosinglets $\tilde{\mathrm{t}}_R$ and $\tilde{\mathrm{b}}_R$. They can be different for each generation, but for simplicity we will assume equal values for all generations in our numerical analysis. $A_t$ and $A_b$ are the parameters of the soft-breaking scalar three-point interactions of top- and bottom-squarks with the Higgs fields.

We restrict our analysis to real parameters. Therefore the mass matrices for $\tilde{\mathrm{t}}$ and $\tilde{\mathrm{b}}$ are real and can be diagonalized by means of rotations with angles $\theta_{\tilde{\mathrm{t}}}$ and $\theta_{\tilde{\mathrm{b}}}$. The mass eigenstates $\tilde{\mathrm{t}}_1$ and $\tilde{\mathrm{t}}_2$ are obtained as

$$\begin{pmatrix} \tilde{\mathrm{t}}_1 \\ \tilde{\mathrm{t}}_2 \end{pmatrix} = \begin{pmatrix} \cos\theta_{\tilde{\mathrm{t}}} & -\sin\theta_{\tilde{\mathrm{t}}} \\ \sin\theta_{\tilde{\mathrm{t}}} & \cos\theta_{\tilde{\mathrm{t}}} \end{pmatrix} \begin{pmatrix} \tilde{\mathrm{t}}_L \\ \tilde{\mathrm{t}}_R \end{pmatrix} ,$$

and analogously for $\tilde{\mathrm{b}}_1$ and $\tilde{\mathrm{b}}_2$.

For the pair production of charged Higgs particles via gluon fusion all couplings of charged and neutral CP-even Higgs particles to squarks appear at leading order. The couplings for mass eigenstates are listed in Appendix C.

## 3 The parton process $gg \to H^-H^+$

The production of charged Higgs pairs by gluon fusion in the MSSM is a loop-induced process, at leading (1-loop) order mediated through quark and squark loops. The Feynman graphs are depicted in Appendix D.

In our kinematical conventions, the momenta of the initial and final state particles are all chosen as incoming:

$$g(p_1,a,\lambda) + g(p_2,b,\lambda') \to H^-(-p_3) + H^+(-p_4)\,.$$

Besides by their momenta, the initial state gluons are characterized by their colour indices $a, b$ and their helicities $\lambda, \lambda'$. We make use of the parton kinematical invariants

$$\hat{s} = (p_1+p_2)^2\,, \quad \hat{t} = (p_1+p_3)^2\,, \quad \hat{u} = (p_1+p_4)^2$$

obeying the relation

$$\hat{s} + \hat{t} + \hat{u} = 2m^2_{H^\pm} \quad .$$

The spin- and colour-averaged cross section for the parton process

$$\frac{d\sigma}{d\hat{t}} = \frac{1}{16\pi\hat{s}^2}\,\frac{1}{4}\sum_{\lambda,\lambda'=\pm1}\frac{1}{64}\sum_{a,b=1}^{8}\left|\mathcal{M}^{ab}_{\lambda\lambda'}\right|^2 \tag{6}$$

contains the helicity amplitudes

$$\mathcal{M}^{ab}_{\lambda\lambda'} = \varepsilon^\mu_{a\lambda}(p_1)\varepsilon^\nu_{b\lambda'}(p_2)\,\widetilde{\mathcal{M}}_{\mu\nu}\cdot(4\pi\alpha_S)\,\mathrm{Tr}\left\{\frac{\lambda^a}{2}\frac{\lambda^b}{2}\right\} \quad , \tag{7}$$

where a pure QCD factor is written separately. The remaining tensor $\widetilde{\mathcal{M}}_{\mu\nu}$ can be decomposed with respect to a complete set of orthogonal tensors $A_i^{\mu\nu}$ [8,9] according to

$$\widetilde{\mathcal{M}}^{\mu\nu} = \sum_{i=1}^{4} F_i(\hat{s},\hat{t})A_i^{\mu\nu}(\hat{s},\hat{t}) \quad . \tag{8}$$

The explicit formulae for the basic tensors are listed in Appendix A. The tensor $\widetilde{\mathcal{M}}_{\mu\nu}$ is transverse:

$$p_1^\mu\widetilde{\mathcal{M}}_{\mu\nu} = 0\,, \quad p_2^\nu\widetilde{\mathcal{M}}_{\mu\nu} = 0 \quad , \tag{9}$$

[2] Our sign convention for $\mu$ is opposite to that of [7]

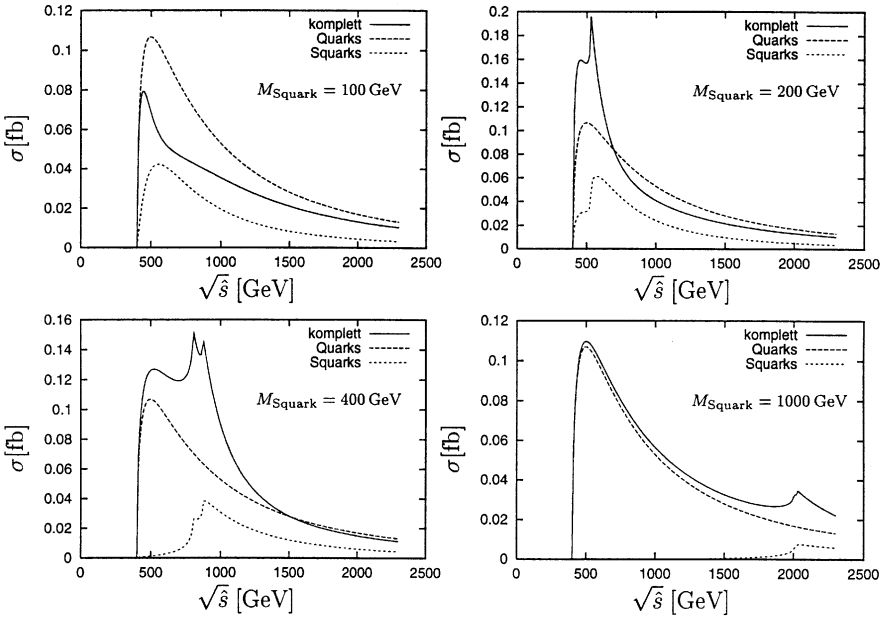


**Fig. 1.** Parton cross section for the production of charged Higgs pairs ($m_{H^\pm} = 200\,\text{GeV}$,$\tan\beta = 1.5$) via gluon fusion for rising values of the common squark mass scale (100/200/400/1000 GeV). The cross section is evaluated with all Feynman graphs (solid lines), only quark loop graphs (long dashed) and only squark loop graphs (short dashed)

and the $A_i^{\mu\nu}$ are chosen to be individually transverse as well. This transversality guarantees that the spin-averaged cross section is proportional to $\widetilde{\mathcal{M}}^{\mu\nu}\widetilde{\mathcal{M}}^{\star}_{\mu\nu}$ and, together with the orthogonality of the basis tensors, that the differential cross section for the parton process can be expressed in a simple way in terms of the form factors:

$$\frac{d\sigma}{d\hat{t}} = \frac{\pi\alpha_S^2}{64\,\hat{s}^2}\sum_{i=1}^{4}\left|F_i(\hat{s},\hat{t})\right|^2 \quad . \tag{10}$$

The form factors can be divided into contributions from loop diagrams with virtual squarks ($\tilde{\text{q}}$) and quarks (q) arising in 2-, 3- and 4-point integrals (denoted by the symbols $\circ$ for 2, $\triangle$ for 3, and $\square$ for 4 internal lines):

$$\begin{aligned} F_1 &= F^{\tilde{\text{q}},\circ} + F^{\tilde{\text{q}},\triangle} + F^{\tilde{\text{q}},\square} + F^{\text{q},\triangle} + F^{\text{q},\square} \\ F_2 &= G^{\tilde{\text{q}},\circ} + G^{\tilde{\text{q}},\triangle} + G^{\tilde{\text{q}},\square} + G^{\text{q},\square} \\ F_3 &= 0 \\ F_4 &= H^{\text{q},\square} \quad . \end{aligned} \tag{11}$$

The tensor $A_3^{\mu\nu}$ projects on a CP-odd gluon state with a total spin component = 0 along the collision axis in the CMS. Since the final state is CP-even for this spin configuration, $F_3$ vanishes identically. Analytic formulae for the form factors in terms of scalar 3- and 4-point-functions are presented in Appendix B. The analytic formulae for the form factors of the quark loop graphs are in agreement with [3]. For a complete and coherent documentation they are also included in Appendix B.

The integrated parton cross section

$$\sigma_{gg\to H^+H^-}(\hat{s},\alpha_S(\mu_R)) = \int_{\hat{t}_{\min}(\hat{s})}^{\hat{t}_{\max}(\hat{s})} d\hat{t}\,\frac{d\sigma}{d\hat{t}} \tag{12}$$

is evaluated by numerical integration over the kinematically allowed $\hat{t}$-range for a given CMS-energy $\sqrt{\hat{s}}$ of the gluon-gluon system. The renormalization scale $\mu_R$ in the strong coupling constant is chosen as $\sqrt{\hat{s}}$, the hard energy scale of the process.

In Fig. 1 the parton cross section is displayed for unmixed squarks ($A = \mu = 0$) for four characteristic values of the squark mass scale which we assume to be common for the various entries in the mass matrices: $M_{\tilde{Q}} = M_{\tilde{U}} = M_{\tilde{D}} =: M_{\text{squark}}$. The parameters of the Higgs sector are $m_{H^\pm} = 200\,\text{GeV}$ and $\tan\beta = 1.5$. The Figure contains a sequence of graphs with rising values of the squark mass scale, beginning with squark masses below $m_{H^\pm}$, then slightly above $m_{H^\pm}$, followed by squark masses around $2m_{H^\pm}$, and finally at 1000 GeV. The decoupling property of heavy squarks is clearly visible, but it also becomes clear that squarks of intermediate mass scales can give rise to a sizeable enhancement of the cross section. Due to significant interferences, the cross sections including both quark and squark loops are not simply the sum of the individual contributions. The spikes in the plots correspond to the squark pair thresholds of the loop diagrams.

## 4 The hadron process $pp \to H^-H^+ + X$

### 4.1 Total hadronic cross section

The hadronic cross section for $H^\pm$ pair production from gluons in proton-proton collisions at a total hadronic CMS energy $\sqrt{S}$ can be written as a convolution [10]

$$\begin{aligned} \sigma &\equiv \sigma(pp \to H^+H^- + X) \\ &= \int_{\tau_0}^{1} d\tau \frac{d\mathcal{L}_{gg}^{pp}}{d\tau}\,\sigma_{gg\to H^+H^-}(\tau S,\alpha_S(\mu_R)) \end{aligned} \tag{13}$$

with the gluon luminosity

$$\frac{d\mathcal{L}_{gg}^{pp}}{d\tau} = \int_{\tau}^{1}\frac{dx}{x} f_{g/p}(x,\mu_F) f_{g/p}(\frac{\tau}{x},\mu_F)\,, \tag{14}$$

where $f_{g/p}(x, \mu_F)$ denotes the density of gluons in the proton carrying a fraction $x$ of the proton momentum at the scale $\mu_F$. The numerical evaluation has been carried out with the MRS(G) gluon distribution functions [11] and with the renormalization and factorization scale $\mu_R, \mu_F$ chosen as equal.

Table 1 collects a sample of numerical results for the hadronic cross section for typical sets of MSSM parameters. Quark masses are $m_t = 175\,\text{GeV}$, $m_b = 5\,\text{GeV}$. We always assume a common squark mass scale $M_{\text{squark}}(= M_{\tilde{Q}} = M_{\tilde{U}} = M_{\tilde{D}})$, which in Table 1 has been set to 200 GeV (where the squark diagrams give a big contribution) and to infinity describing the case of decoupling squarks. An unmixed squark mass scenario is assumed ($A = \mu = 0$). $\tan\beta = 6$ is chosen as a reference point for the minimal cross section (see also Fig. 7), and $\tan\beta = 50$ as a representative value for the large $\tan\beta$ scenario.

Cross sections and numbers of events in Table 1 are given for the projected collider energies and integrated luminosities of LHC and Tevatron Run II. At the Tevatron, the gluon fusion mechanism for charged Higgs pair production is irrelevant. Therefore, for the subsequent discussions we will focus on the LHC with $\sqrt{S} = 14$ TeV.

The variation of the cross section with the MSSM parameter $\mu$ is displayed in Fig. 2. Except for $\tan\beta$ values around the minimum of the cross section, the $\mu$-dependence is very flat and the choice $\mu = 0$ already illustrates the typical size of the cross section very well. For $\tan\beta = 1.5$ a sizeable increase occurs for larger values of $|\mu|$ by an order of magnitude, but still far below the high $\tan\beta$ scenario.

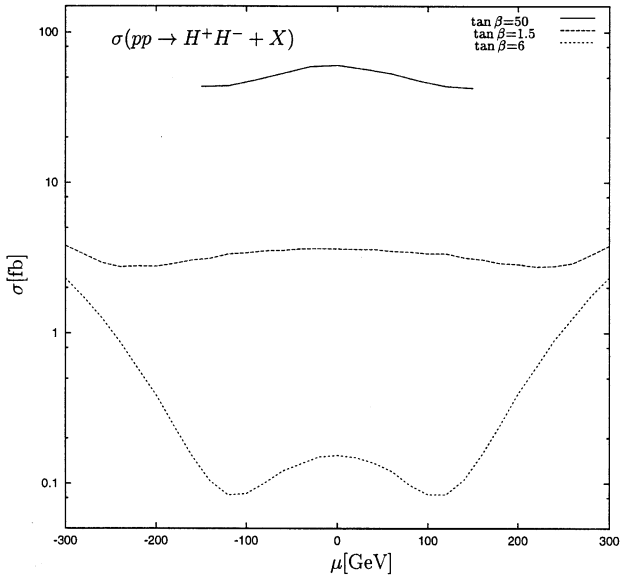


**Fig. 2.** $\mu$-dependence of the hadronic cross section for $m_{H^\pm} = M_{\text{squark}} = 200\,\text{GeV}$ and $A_t = 0$ and for three values of $\tan\beta$ (1.5/6/50). For $\tan\beta = 50$ the graph is not extended over the full range because one of the stop masses would become too light

## 4.2 Dependence on the Higgs parameters

The input parameters for the Higgs sector are $m_{H^\pm}$ and $\tan\beta$. Figure 3 shows the dependence of the hadronic cross section (13) on the mass of the charged Higgs for three representative values of $\tan\beta$ (including the minimum at $\tan\beta \approx 6$). The common squark mass scale is $M_{\text{squark}} = 200\,\text{GeV}$ and all squark mixing is switched off ($A_t = A_b = \mu = 0$). The hadronic cross section decreases almost exponentially with rising $m_{H^\pm}$. This behaviour is essentially explained by the decreasing number of gluons at large values of $x$. For Higgs masses near $m_t$, the top threshold gives rise to a step with a slight increase of $\sigma$.

The dashed lines in Fig. 3 show the cross section for decoupling squarks. The difference demonstrates the large effect squarks can have on the cross section whenever they are not too heavy. In the special case of $m_{H^\pm} = 170\,\text{GeV}$ and $\tan\beta = 6$ the cross section is more than 3 times the decoupling limit and even for $M_{\text{squark}} = 500\,\text{GeV}$ the cross section is still 15 % higher than in the decoupling case, independent of $\tan\beta$ and for charged Higgs masses in the range of Fig. 3.

The variation of the hadronic cross section with $\tan\beta$ is displayed in Fig. 7. The cross section has a pronounced minimum at

$$\tan\beta \approx \sqrt{\frac{m_t}{m_b}} \approx 6 \quad ,$$

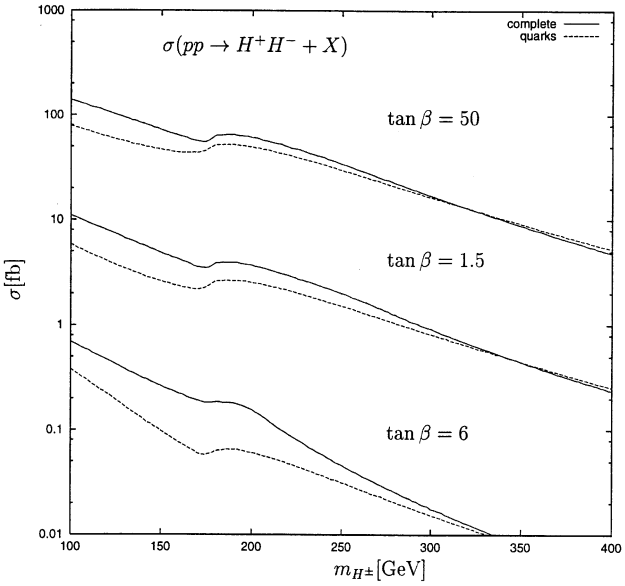


**Fig. 3.** Variation of the hadronic cross section (solid lines) with the mass of the charged Higgs particle for three values of $\tan\beta$ (6/1.5/50) and a squark mass scale of $M_{\text{squark}} = 200\,\text{GeV}$. Additionally the contribution of only the quark loops to the cross section is depicted (dashed lines), which corresponds to the limit of large squark masses

**Table 1.** Cross section for charged Higgs pair production via gluon fusion in $pp$ ($p\bar{p}$) collisons for hadron energies of 2 and 14 TeV, corresponding to the Tevatron and LHC. Additionally the number of events in one year of running is given, assuming $2\,\mathrm{fb}^{-1}$ of integrated lumiosity for the Tevatron and $100\,\mathrm{fb}^{-1}$ for the LHC

| $\tan\beta$ | $m_{H^\pm}$ [GeV] | $M_{\mathrm{squark}}$ [GeV] | $\sqrt{S} = 14$ TeV | | $\sqrt{S} = 2$ TeV | |
|---|---|---|---|---|---|---|
| | | | $\sigma$ [fb] | events | $\sigma$ [fb] | events |
| 50 | 100 | 200 | 140.7 | $\approx 14000$ | 0.48 | $\approx 1$ |
| | | $\infty$ | 79.7 | $\approx 7900$ | 0.26 | $\approx 0.5$ |
| | 200 | 200 | 60.7 | $\approx 6000$ | $5.4{\cdot}10^{-2}$ | $\approx 0.1$ |
| | | $\infty$ | 49.4 | $\approx 5000$ | $3.7{\cdot}10^{-2}$ | - |
| 6 | 100 | 200 | 0.71 | 71 | $3.2{\cdot}10^{-3}$ | - |
| | | $\infty$ | 0.38 | 38 | $2.1{\cdot}10^{-3}$ | - |
| | 200 | 200 | 0.16 | 16 | $1.7{\cdot}10^{-4}$ | - |
| | | $\infty$ | $6.0{\cdot}10^{-2}$ | 6 | $5.4{\cdot}10^{-5}$ | - |

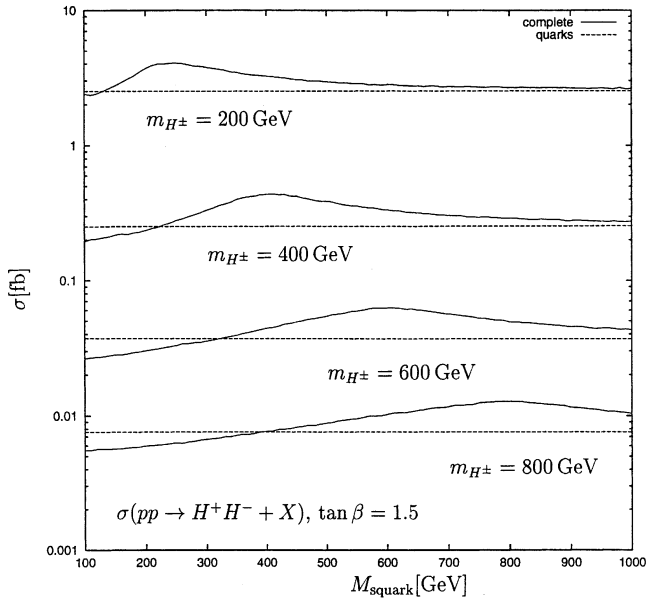


**Fig. 4.** Hadronic cross section for different values of $m_{H^\pm}$ ($200/400/600/800\,GeV$) versus the squark mass scale $M_{\mathrm{squark}}$ with $\tan\beta = 1.5$ (solid lines). For comparison the contribution of only the quark loops is displayed in terms of the horizontal dashed lines

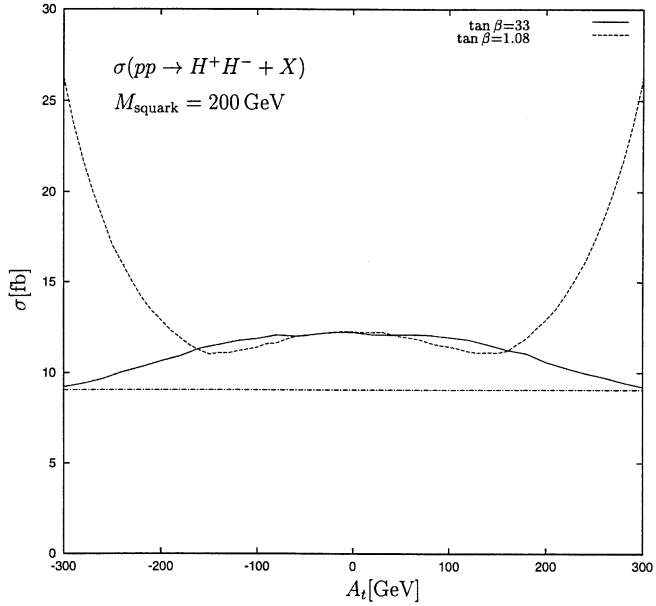


**Fig. 5.** Hadronic cross section for $m_{H^\pm} = 200\,\mathrm{GeV}$ and two values of $\tan\beta$ (33: solid, 1.08: dashed) versus the mixing parameter $A_t$. For comparison the dot-dashed line shows the cross section for $\tan\beta = 1.08$ with the pure fermion loop contribution

which is a consequence of the $\tan\beta$-dependence of the quark and squark couplings to charged Higgs bosons.

### 4.3 Dependence on the squark sector

The contribution of the squark loop graphs (Appendix D.1) to the cross sections vanishes for large squark masses, due to the decoupling property of the scalar quarks, and the pure fermion loop result of [3] is recovered (see Fig. 4). The squark contribution is especially significant for squark masses close to $m_{H^\pm}$, where the parton cross section near the Higgs production threshold is enhanced by about a factor of 2 compared to the cross section from quark loops only (see Fig. 1). For squark masses lower than $m_{H^\pm}$, the squark loop amplitudes interfere mainly destructively with the quark loop amplitudes, thus diminishing the cross section as compared to the decoupling case.

The predominant squark contribution comes from the third generation with their large Yukawa couplings. The structure of these couplings gives rise to the minimum behaviour of $\sigma$ as a function of $\tan\beta$. There are, however, also squark couplings independent of the quark masses and hence not suppressed by light quark masses for the two other generations (see Appendix C). These contributions, although much smaller in size, are not completely negligible: for $\tan\beta \sim 6$ they constitute 45% of the cross section. Since they are essentially $\tan\beta$ independent, their relative influence decreases at other values of $\tan\beta$ with larger cross sections.

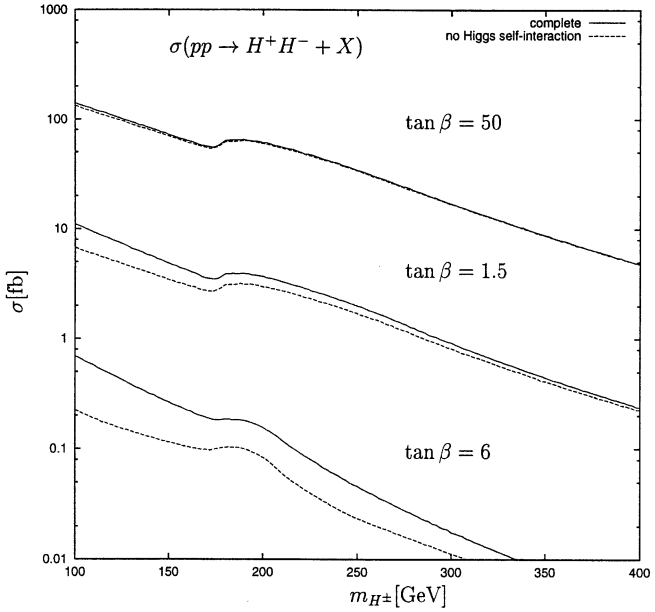


**Fig. 6.** Comparison between the hadronic cross section versus the charged Higgs mass with and without the trilinear Higgs coupling (solid and dashed line, respectively) for three values of $\tan\beta$ (6/1.5/50). The squark mass scale is $M_{\text{squark}} = 200\,\text{GeV}$

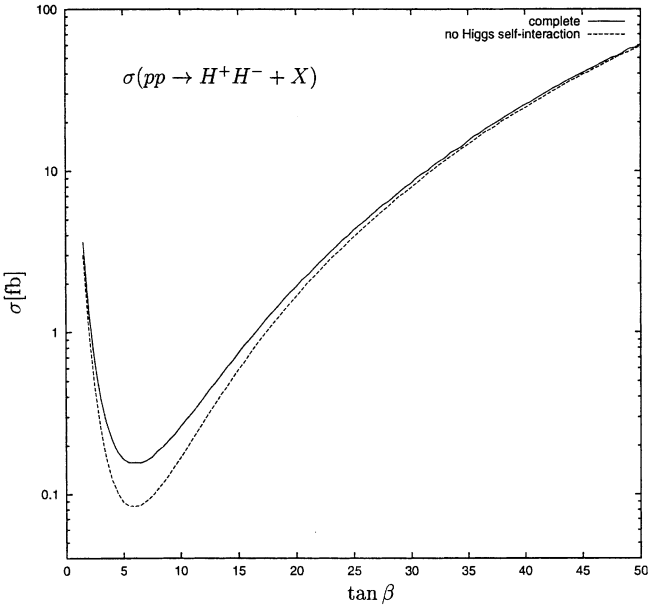


**Fig. 7.** Variation of the hadronic cross section with $\tan\beta$ calculated with (solid line) and without (dashed line) the trilinear Higgs couplings. The mass of the charged Higgs is $m_{H^\pm} = 200\,\text{GeV}$ and the squark mass scale is $M_{\text{squark}} = 200\,\text{GeV}$

The effects of mixing in the stop sector are visualized in Fig. 5, where the non-diagonal entry $A_t$ in the stop mass matrix is varied (for $\mu = 0$), for two $\tan\beta$-values (1.08 and 33). For small values of $A_t$, the cross sections are nearly identical. In the low $\tan\beta$ case, however, a significantly higher cross section can be obtained by increasing the value of $A_t$, with a strong dependence on $A_t$.

### 4.4 Sensitivity to the Higgs self interaction

Analogously to the standard Higgs case [8] one may ask wether charged Higgs pair production is sensitive to the Higgs self interaction that enters through the neutral Higgs exchange graphs (see Appendix D.1). The situation here is less transparent than in the standard model because of the two neutral Higgs particles with different couplings to the charged Higgs pair.

To illustrate the influence of the Higgs self interaction, Figs. 6 and 7 show the complete cross section (solid lines) versus the cross section evaluated with the Higgs self interaction turned off (dashed lines). In both figures the same squark mass scenario as in chapter 4.2 has been adopted (i.e. $M_{\text{squark}} = 200\,\text{GeV}$ and no squark mixing). Except around the minimum, the relative contribution of the Higgs self interaction is much smaller than the contributions from the box diagrams (the observation of the smallness of the diagrams with the quark/squark triangles has already been made in [2]).

## 5 Conclusions

Gluon-gluon fusion is an important mechanism for producing charged Higgs particles at the LHC. Although at smaller rates than in $q\bar{q}$ annihilation, it is sensitive also to the scalar quark sector if the Higgs bosons are supersymmetric. For not too large masses, virtual squarks are not negligible and can increase the cross section up to a factor 2, in special cases even 3, compared to the decoupling limit with heavy squarks. For squark masses not smaller than $m_{H^\pm}$ the squark contribution is always positive. An interesting behaviour is observed for squark mixing: For low values of $\tan\beta$ the cross section is strongly dependent on the trilinear top squark coupling $A_t$, yielding a steep rise for increasing values of $A_t$. Charged Higgs boson pairs can thus provide a valuable source of information, useful to disentangle various classes of models.

*Acknowledgement.* We would like to thank A. Barrientos and B. Kniehl for helpful discussions.

## A Tensor basis

The amplitude $\mathcal{M}^{fi}_{\lambda\lambda'}$ for the fusion of two massless vector particles into two scalar particles is decomposed as follows:

$$\mathcal{M}^{fi}_{\lambda\lambda'} = N_{fi}\,\varepsilon^{\mu}_{\lambda}(p_1)\varepsilon^{\nu}_{\lambda'}(p_2)\widetilde{\mathcal{M}}_{\mu\nu} \quad , \quad \widetilde{\mathcal{M}}_{\mu\nu} = \sum_{i=1}^{4} F_i A_i^{\mu\nu} \quad ,$$

with a normalization factor $N_{fi}$ and the following tensor basis [8,9]:

$$A_1^{\mu\nu} = g^{\mu\nu} - \frac{p_2^{\mu}p_1^{\nu}}{p_1 p_2} \tag{15}$$

$$A_2^{\mu\nu} = g^{\mu\nu} + \frac{p_3^2 p_2^\mu p_1^\nu}{p_t^2(p_1p_2)} - \frac{2(p_2p_3)p_3^\mu p_1^\nu}{p_t^2(p_1p_2)} - \frac{2(p_1p_3)p_2^\mu p_3^\nu}{p_t^2(p_1p_2)} + \frac{2p_3^\mu p_3^\nu}{p_t^2} \tag{16}$$

$$A_3^{\mu\nu} = \frac{\epsilon^{\mu\nu p_1 p_2}}{(p_1p_2)} \tag{17}$$

$$A_4^{\mu\nu} = \Big\{ p_3^\mu \epsilon^{\nu p_1 p_2 p_3} + p_3^\nu \epsilon^{\mu p_1 p_2 p_3} + (p_2p_3)\epsilon^{\mu\nu p_1 p_3} + (p_1p_3)\epsilon^{\mu\nu p_2 p_3} \Big\} \Big/ \Big\{ p_t^2 (p_1p_2) \Big\} \quad . \tag{18}$$

The transverse momentum squared $p_t^2$ is defined as

$$p_t^2 = 2\frac{(p_1p_3)(p_2p_3)}{(p_1p_2)} - p_3^2 \quad .$$

The properties of these tensors, which have been exploited in the calculation, are tranversality:

$$p_{1,\mu} A_i^{\mu\nu} = 0\,, \quad p_{2,\nu} A_i^{\mu\nu} = 0$$

and orthogonality:

$$A_i^{\mu\nu} A_{j,\mu\nu} = 2\,\delta_{ij} \quad .$$

## B Form factors

For 3- and 4-point functions the following shorthand notations are defined:

$$C_{lm}^{ABC} = \frac{1}{i\pi^2} \int d^4k \Big\{ 1 \Big\} \Big/ \Big\{ \left[k^2 - m_A^2\right] \left[(k+p_l)^2 - m_B^2\right] \times \left[(k+p_l+p_m)^2 - m_C^2\right] \Big\} \quad ,$$

$$D_{klm}^{ABCD} = \frac{1}{i\pi^2} \int d^4k \Big\{ 1 \Big\} \Big/ \Big\{ \left[k^2 - m_A^2\right] \left[(k+p_k)^2 - m_B^2\right] \times \left[(k+p_k+p_l)^2 - m_C^2\right] \times \left[(k+p_k+p_l+p_m)^2 - m_D^2\right] \Big\} \quad .$$

### B.1 Squark contributions

The form factors from squark loops with two or three internal lines are:

$$F_{\tilde{\mathrm{q}}}^{\circ} + F_{\tilde{\mathrm{q}}}^{\triangle} = \frac{1}{4\pi^2} \sum_{l,k=1}^{2} \left[ f_{\tilde{\mathrm{q}},1}^{\circ+\triangle}(l,k) + f_{\tilde{\mathrm{q}},2}^{\circ+\triangle}(l,k) \right] \tag{19}$$

with

$$f_{\tilde{\mathrm{q}},1}^{\circ+\triangle}(l,k) = \sum_{\tilde{\mathrm{q}}=\tilde{\mathrm{t}},\tilde{\mathrm{b}}} \left[ \delta_{lk} \left( \frac{1}{2} + m_{\tilde{\mathrm{q}}_l}^2 C_{12}^{\tilde{\mathrm{q}}_l\tilde{\mathrm{q}}_l\tilde{\mathrm{q}}_l} \right) \times \left( g[\tilde{\mathrm{q}}_l, \tilde{\mathrm{q}}_l, H^+, H^-] - \sum_{i=1}^{2} \frac{g[H_i^0, H^+, H^-]\, g[H_i^0, \tilde{\mathrm{q}}_l, \tilde{\mathrm{q}}_l]}{s - m_{H_i^0}^2} \right) \right] \tag{20}$$

$$f_{\tilde{\mathrm{q}},2}^{\circ+\triangle}(l,k) = \tfrac{3}{4} V_{lk} \left( C_{34}^{\tilde{\mathrm{t}}_k\tilde{\mathrm{b}}_l\tilde{\mathrm{t}}_k} + C_{34}^{\tilde{\mathrm{b}}_l\tilde{\mathrm{t}}_k\tilde{\mathrm{b}}_l} \right) \quad , \tag{21}$$

and

$$G_{\tilde{\mathrm{q}}}^{\circ} + G_{\tilde{\mathrm{q}}}^{\triangle} = \frac{1}{4\pi^2} \sum_{l,k=1}^{2} V_{lk} \left[ \frac{1}{4} \left( 2 + \frac{m_{H^\pm}^2}{p_t^2} \right) \times \left( C_{34}^{\tilde{\mathrm{t}}_k\tilde{\mathrm{b}}_l\tilde{\mathrm{t}}_k} + C_{34}^{\tilde{\mathrm{b}}_l\tilde{\mathrm{t}}_k\tilde{\mathrm{b}}_l} \right) \right] \quad . \tag{22}$$

$V_{lk}$ is a shorthand notation for the product of two couplings of squarks to the charged Higgs particle which appears again in the box amplitudes:

$$V_{lk} = g[H^\pm, \tilde{\mathrm{t}}_k, \tilde{\mathrm{b}}_l]^2 \quad . \tag{23}$$

The form factors originating from squark box diagramms are:

$$F_{\tilde{\mathrm{q}}}^{\Box} = \frac{1}{4\pi^2} \sum_{l,k=1}^{2} V_{lk} \Big[ \big( f_{\tilde{\mathrm{q}}}^{\Box}(\tilde{\mathrm{t}}_k, \tilde{\mathrm{b}}_l; \hat{t}, \hat{u}) + f_{\tilde{\mathrm{q}}}^{\Box}(\tilde{\mathrm{b}}_l, \tilde{\mathrm{t}}_k; \hat{t}, \hat{u}) \big) + \big( \hat{t} \leftrightarrow \hat{u} \big) \Big] \tag{24}$$

with

$$f_{\tilde{\mathrm{q}}}^{\Box}(\tilde{\mathrm{t}}_k, \tilde{\mathrm{b}}_l; \hat{t}, \hat{u}) = \frac{(\hat{t} - m_{H^\pm}^2)}{2\,\hat{s}} C_{13}^{\tilde{\mathrm{t}}_k\tilde{\mathrm{t}}_k\tilde{\mathrm{b}}_l} - \frac{3}{8} C_{34}^{\tilde{\mathrm{t}}_k\tilde{\mathrm{b}}_l\tilde{\mathrm{t}}_k} - \frac{m_{\tilde{\mathrm{t}}_k}^2}{2} D_{123}^{\tilde{\mathrm{t}}_k\tilde{\mathrm{t}}_k\tilde{\mathrm{t}}_k\tilde{\mathrm{b}}_l} - \frac{m_{\tilde{\mathrm{t}}_k}^2 + m_{\tilde{\mathrm{b}}_l}^2 + p_t^2}{8} D_{132}^{\tilde{\mathrm{t}}_k\tilde{\mathrm{t}}_k\tilde{\mathrm{b}}_l\tilde{\mathrm{b}}_l} \quad , \tag{25}$$

and

$$G_{\tilde{\mathrm{q}}}^{\Box} = \frac{1}{4\pi^2} \sum_{l,k=1}^{2} V_{lk} \Big[ \big( g_{\tilde{\mathrm{q}}}^{\Box}(\tilde{\mathrm{t}}_k, \tilde{\mathrm{b}}_l; \hat{t}, \hat{u}) + g_{\tilde{\mathrm{q}}}^{\Box}(\tilde{\mathrm{b}}_l, \tilde{\mathrm{t}}_k; \hat{t}, \hat{u}) \big) + \big( \hat{t} \leftrightarrow \hat{u} \big) \Big] \tag{26}$$

with

$$g_{\tilde{\mathrm{q}}}^{\Box}(\tilde{\mathrm{t}}_k, \tilde{\mathrm{b}}_l; \hat{t}, \hat{u}) = \frac{1}{2p_t^2} \Bigg[ \frac{1}{2} \left( m_{\tilde{\mathrm{t}}_k}^2 - m_{\tilde{\mathrm{b}}_l}^2 + m_{H^\pm}^2 - \frac{\hat{s}}{2} \right) C_{12}^{\tilde{\mathrm{t}}_k\tilde{\mathrm{t}}_k\tilde{\mathrm{t}}_k} + \frac{\hat{t}\,(\hat{t} - m_{H^\pm}^2)}{\hat{s}} C_{13}^{\tilde{\mathrm{t}}_k\tilde{\mathrm{t}}_k\tilde{\mathrm{b}}_l} + \frac{1}{4}(3m_{H^\pm}^2 - \hat{s}) C_{34}^{\tilde{\mathrm{t}}_k\tilde{\mathrm{b}}_l\tilde{\mathrm{t}}_k} - \frac{1}{4} \left( (m_{\tilde{\mathrm{t}}_k}^2 + m_{\tilde{\mathrm{b}}_l}^2) p_t^2 + (m_{\tilde{\mathrm{t}}_k}^2 - m_{\tilde{\mathrm{b}}_l}^2)^2 \right) D_{132}^{\tilde{\mathrm{t}}_k\tilde{\mathrm{t}}_k\tilde{\mathrm{b}}_l\tilde{\mathrm{b}}_l} - \frac{1}{2} \Bigg( (\hat{t} - m_{\tilde{\mathrm{b}}_l}^2)^2 + m_{\tilde{\mathrm{t}}_k}^2 \Bigg( m_{\tilde{\mathrm{t}}_k}^2 - 2m_{\tilde{\mathrm{b}}_l}^2 - 2\frac{(\hat{t} - m_{H^\pm}^2)^2}{\hat{s}} \Bigg) \Bigg) D_{213}^{\tilde{\mathrm{t}}_k\tilde{\mathrm{t}}_k\tilde{\mathrm{t}}_k\tilde{\mathrm{b}}_l} \Bigg] \quad . \tag{27}$$

### B.2 Quark contributions

The form factor due to triangle quark loops is:

$$F_{\rm q}^{\triangle} = \frac{1}{4\pi^2}\sum_{i=1}^{2}\left[f_{\rm q}^{\triangle}(H_i^0,t)+f_{\rm q}^{\triangle}(H_i^0,b)\right] \tag{28}$$

with

$$f_{\rm q}^{\triangle}(H_i^0,q) = \frac{g[H_i^0,q,q]\,g[H_i^0,H^+,H^-]}{\hat{s}-m_{H_i^0}^2+im_{H_i^0}\Gamma_{H_i^0}}m_q \times\Big(2+(4m_q^2-\hat{s})C_{12}^{qqq}\Big)\quad , \tag{29}$$

and the form factors from quark box graphs are:

$$\begin{aligned}F_{\rm q}^{\Box} = \frac{1}{4\pi^2}\Bigg[&\Big(g_s[H^\pm,t,b]^2\Big(f_{\rm q}^{\Box}(m_t,m_b;\hat{t},\hat{u})\\ &+f_{\rm q}^{\Box}(m_b,m_t;\hat{t},\hat{u})\Big)+g_p[H^\pm,t,b]^2\\ &\times\Big(f_{\rm q}^{\Box}(m_t,-m_b;\hat{t},\hat{u})+f_{\rm q}^{\Box}(m_b,-m_t;\hat{t},\hat{u})\Big)\Big)\\ &+\Big(\hat{t}\leftrightarrow\hat{u}\Big)\Bigg]\end{aligned} \tag{30}$$

with

$$\begin{aligned}&f_{\rm q}^{\Box}(m_t,m_b;\hat{t},\hat{u})\\ &=\frac{1}{2}+m_t^2C_{12}^{ttt}+\big(m_{H^\pm}^2-(m_t+m_b)^2\big)\frac{(\hat{t}-m_{H^\pm}^2)}{\hat{s}}C_{13}^{ttb}\\ &\quad -m_tm_b\frac{\hat{s}}{4}(2D_{123}^{tttb}+D_{132}^{ttbb})-\frac{1}{4}\big(m_{H^\pm}^2-(m_t+m_b)^2\big)\\ &\quad\times\Big((p_t^2+m_b^2+m_t^2)D_{132}^{ttbb}+4m_t^2D_{123}^{tttb}\Big)\quad ;\end{aligned} \tag{31}$$

$$\begin{aligned}G_{\rm q}^{\Box} = \frac{1}{4\pi^2}\Bigg[&\Big(g_s[H^\pm,t,b]^2\Big(g_{\rm q}^{\Box}(m_t,m_b;\hat{t},\hat{u})\\ &+g_{\rm q}^{\Box}(m_b,m_t;\hat{t},\hat{u})\Big)+g_p[H^\pm,t,b]^2\Big(g_{\rm q}^{\Box}(m_t,-m_b;\hat{t},\hat{u})\\ &+g_{\rm q}^{\Box}(m_b,-m_t;\hat{t},\hat{u})\Big)\Big)+\Big(\hat{t}\leftrightarrow\hat{u}\Big)\Bigg]\end{aligned} \tag{32}$$

with

$$\begin{aligned}&g_{\rm q}^{\Box}(m_t,m_b;\hat{t},\hat{u})\\ &=\frac{1}{4p_t^2}\Bigg[\left(\frac{\hat{s}}{2}+(m_t+m_b)^2-m_{H^\pm}^2\right)\left(\left(2p_t^2+\frac{(\hat{u}-\hat{t})^2}{\hat{s}}\right)\right.\\ &\quad\left.\times C_{34}^{tbt}+\big(2(m_{H^\pm}^2+m_t^2-m_b^2)-\hat{s}\big)C_{12}^{ttt}\right)-\hat{s}p_t^2C_{12}^{ttt}\\ &\quad+2\frac{(\hat{t}-m_{H^\pm}^2)}{\hat{s}}\Big(m_{H^\pm}^4+\hat{t}^2-2\hat{t}(m_t+m_b)^2\Big)C_{13}^{ttb}\\ &\quad+p_t^2\Bigg(\big(\hat{s}m_b^2-2m_t^2(2m_b^2-m_t^2+m_{H^\pm}^2)\big)D_{123}^{tttb}\\ &\quad+\left(\frac{\hat{s}}{2}(m_t^2+m_b^2)+P_1(m_t,m_b,m_{H^\pm})\right)D_{132}^{ttbb}\Bigg)\\ &\quad+m_t^4\frac{(\hat{t}-m_{H^\pm}^2)^2}{\hat{s}}\Big(D_{123}^{tttb}-3D_{213}^{tttb}\Big)-\frac{\hat{u}}{\hat{s}}m_t^2(\hat{t}^2-m_{H^\pm}^4)\\ &\quad\times(D_{123}^{tttb}+D_{213}^{tttb})-2\Big(m_b^2m_t^2\frac{(\hat{t}-\hat{u})^2}{\hat{s}}\\ &\quad-P_2(m_t,m_b,m_{H^\pm})\Big)D_{123}^{tttb}+\Big(-\hat{t}^3+4\hat{t}^2m_b(m_t+m_b)\\ &\quad-\hat{t}(8m_b^3m_t+4m_b^4+m_{H^\pm}^4)+8m_bm_t^3\Big((\hat{t}-\hat{u})\\ &\quad-\frac{(\hat{u}-m_{H^\pm}^2)^2}{\hat{s}}\Big)+(\hat{s}-2m_{H^\pm}^2)m_b^4\Big)D_{213}^{tttb}\\ &\quad+\frac{1}{2}(m_t^2-m_b^2)^2\Big(2(m_{H^\pm}^2+(m_t+m_b)^2)\\ &\quad+\frac{(\hat{u}-\hat{t})^2}{\hat{s}}\Big)D_{132}^{ttbb}\Bigg]\end{aligned} \tag{33}$$

containing the polynomials

$$\begin{aligned}P_1(m_t,m_b,m_{H^\pm}) = 3m_t^4+2m_t^3m_b-2m_t^2m_b^2+2m_tm_b^3\\ +3m_b^4-m_{H^\pm}^2(m_t^2+m_b^2)\end{aligned} \tag{34}$$

$$\begin{aligned}&P_2(m_t,m_b,m_{H^\pm})\\ &=m_t^6+2m_t^5m_b-m_t^4m_b^2-4m_t^3m_b^3-m_t^2m_b^4+2m_tm_b^5\\ &\quad+m_b^6-m_{H^\pm}^4(m_t^2-m_b^2)-2m_{H^\pm}^2m_t^2m_b^2\quad ;\end{aligned} \tag{35}$$

$$\begin{aligned}H_{\rm q}^{\Box} = \frac{1}{4\pi^2}g_s[H^\pm,t,b]g_p[H^\pm,t,b]\Big[\big(h_{\rm q}^{\Box}(m_t,m_b;\hat{t},\hat{u})\\ +h_{\rm q}^{\Box}(m_b,m_t;\hat{t},\hat{u})\big)-\big(\hat{t}\leftrightarrow\hat{u}\big)\Big]\end{aligned} \tag{36}$$

with

$$\begin{aligned}&h_{\rm q}^{\Box}(m_t,m_b;\hat{t},\hat{u})\\ &=\frac{1}{2p_t^2}\Bigg[\hat{t}\Big((\hat{s}-2m_{H^\pm}^2+2m_b^2-2m_t^2)C_{12}^{ttt}\\ &\quad+(\hat{s}-4m_{H^\pm}^2)C_{34}^{tbt}\Big)-2\frac{(\hat{t}-m_{H^\pm}^2)^2}{\hat{s}}(\hat{t}+m_{H^\pm}^2)C_{13}^{ttb}\\ &\quad+p_t^2\hat{t}\Big(m_t^2(D_{123}^{tttb}+D_{213}^{tttb})+(m_t^2+m_b^2)D_{132}^{ttbb}\Big)\\ &\quad+\hat{t}(m_t^2-m_b^2)^2\Big(D_{123}^{tttb}+D_{213}^{tttb}+D_{132}^{ttbb}\Big)\\ &\quad+\Bigg(2\frac{(\hat{u}-m_{H^\pm}^2)}{\hat{s}}(\hat{t}-\hat{u})m_t^2m_{H^\pm}^2+(\hat{u}^2-m_{H^\pm}^4)\\ &\quad\times\left(2\frac{(\hat{u}-m_{H^\pm}^2)}{\hat{s}}m_t^2-\hat{u}+2m_b^2\right)-\hat{s}p_t^2m_b^2\Bigg)D_{123}^{tttb}\Bigg].\end{aligned} \tag{37}$$

## C MSSM couplings

In the following all couplings of third generation quarks and squarks to MSSM Higgs particles, that are relevant to

the process, are collected. The factor $g_2 = e/s_w$ denotes the coupling constant of the weak interaction, $s_w = \sin\theta_w$, $c_w = \cos\theta_w$ and $t_w = \tan\theta_w$ with the weak mixing angle $\theta_w$. The subscripts 's' and 'p' in $g_s[\cdots]$ and $g_p[\cdots]$ distinguish between the scalar and pseudoscalar couplings in the Higgs–fermion interactions.

### C.1 Higgs self couplings

$$g[H_1^0, H^+, H^-] = -g_2 \left[ m_W \cos(\beta-\alpha) - \frac{m_Z}{2c_w} \cos 2\beta \cos(\alpha+\beta) \right] \quad , \tag{38}$$

$$g[H_2^0, H^+, H^-] = -g_2 \left[ m_W \sin(\beta-\alpha) + \frac{m_Z}{2c_w} \cos 2\beta \sin(\alpha+\beta) \right] . \tag{39}$$

### C.2 Quark couplings to Higgs bosons

Neutral Higgs bosons

$$\begin{aligned} g_s[H_1^0, t, t] &= -g_2 \frac{m_t}{2m_W} \frac{\sin\alpha}{\sin\beta} \quad , \\ g_s[H_1^0, b, b] &= -g_2 \frac{m_b}{2m_W} \frac{\cos\alpha}{\cos\beta} \quad , \end{aligned} \tag{40}$$

$$\begin{aligned} g_s[H_2^0, t, t] &= -g_2 \frac{m_t}{2m_W} \frac{\cos\alpha}{\sin\beta} \quad , \\ g_s[H_2^0, b, b] &= +g_2 \frac{m_b}{2m_W} \frac{\sin\alpha}{\cos\beta} \quad , \end{aligned} \tag{41}$$

$$g_p[H_i^0, t, t] = 0 \quad , \qquad g_p[H_i^0, b, b] = 0 \quad . \tag{42}$$

Charged Higgs bosons

$$\begin{aligned} g_s[H^+ \text{ out}, t \text{ in}, b \text{ out}] &= g_2 \frac{m_b \tan\beta + m_t \cot\beta}{2\sqrt{2} m_W} \\ &= g_s[H^- \text{ out}, b \text{ in}, t \text{ out}] \end{aligned} \tag{43}$$

$$\begin{aligned} g_p[H^+ \text{ out}, t \text{ in}, b \text{ out}] &= -g_2 \frac{m_b \tan\beta - m_t \cot\beta}{2\sqrt{2} m_W} \\ &= -g_p[H^- \text{ out}, b \text{ in}, t \text{ out}] \end{aligned} \tag{44}$$

### C.3 Squark couplings to Higgs bosons

Neutral Higgs bosons

$$\begin{aligned} &g[H_1^0, \tilde{\mathrm{t}}_1, \tilde{\mathrm{t}}_1] \\ &= g_2 \left[ \frac{m_t}{2m_W \sin\beta} \Big( (A_t \sin\alpha - \mu\cos\alpha) \sin 2\theta_{\tilde{\mathrm{t}}} - 2m_t \sin\alpha \Big) \right. \\ &\quad \left. + \frac{m_Z \cos(\alpha+\beta)}{6c_w} \Big( (5 - 8c_w^2) \cos^2\theta_{\tilde{\mathrm{t}}} - 4s_w^2 \Big) \right] \end{aligned} \tag{45}$$

$$\begin{aligned} &g[H_1^0, \tilde{\mathrm{t}}_2, \tilde{\mathrm{t}}_2] \\ &= g_2 \left[ \frac{m_t}{2m_W \sin\beta} \Big( -(A_t \sin\alpha - \mu\cos\alpha) \sin 2\theta_{\tilde{\mathrm{t}}} \right. \\ &\quad -2m_t \sin\alpha \Big) + \frac{m_Z \cos(\alpha+\beta)}{6c_w} \Big( -(5 - 8c_w^2) \cos^2\theta_{\tilde{\mathrm{t}}} \\ &\quad \left. +(1 - 4s_w^2) \Big) \right] \end{aligned} \tag{46}$$

$$\begin{aligned} &g[H_1^0, \tilde{\mathrm{b}}_1, \tilde{\mathrm{b}}_1] \\ &= g_2 \left[ \frac{m_b}{2m_W \cos\beta} \Big( (A_b \cos\alpha - \mu\sin\alpha) \sin 2\theta_{\tilde{\mathrm{b}}} - 2m_b \cos\alpha \Big) \right. \\ &\quad \left. + \frac{m_Z \cos(\alpha+\beta)}{6c_w} \Big( (4c_w^2 - 1) \cos^2\theta_{\tilde{\mathrm{b}}} + 2s_w^2 \Big) \right] \end{aligned} \tag{47}$$

$$\begin{aligned} &g[H_1^0, \tilde{\mathrm{b}}_2, \tilde{\mathrm{b}}_2] \\ &= g_2 \left[ \frac{m_b}{2m_W \cos\beta} \Big( -(A_b \cos\alpha - \mu\sin\alpha) \sin 2\theta_{\tilde{\mathrm{b}}} \right. \\ &\quad -2m_b \cos\alpha \Big) + \frac{m_Z \cos(\alpha+\beta)}{6c_w} \Big( -(4c_w^2 - 1) \cos^2\theta_{\tilde{\mathrm{b}}} \\ &\quad \left. +(1 + 2c_w^2) \Big) \right] \end{aligned} \tag{48}$$

$$\begin{aligned} &g[H_2^0, \tilde{\mathrm{q}}_i, \tilde{\mathrm{q}}_i] \\ &= g[H_1^0, \tilde{\mathrm{q}}_i, \tilde{\mathrm{q}}_i] \left( \sin\alpha \to \cos\alpha \,,\ \cos\alpha \to -\sin\alpha \right) \end{aligned} \tag{49}$$

Charged Higgs bosons

$$\begin{aligned} &g[H^+ \text{ out}, \tilde{\mathrm{t}}_1 \text{ in}, \tilde{\mathrm{b}}_1 \text{ out}] = g[H^- \text{ out}, \tilde{\mathrm{t}}_1 \text{ out}, \tilde{\mathrm{b}}_1 \text{ in}] \\ &= \frac{g_2}{2\sqrt{2} m_W} \Big[ \sin 2\beta \Big( m_b^2 (1 + \tan^2\beta) + m_t^2 (1 + \cot^2\beta) \\ &\quad -2m_W^2 \Big) \cos\theta_{\tilde{\mathrm{b}}} \cos\theta_{\tilde{\mathrm{t}}} + 2m_t m_b (\tan\beta + \cot\beta) \sin\theta_{\tilde{\mathrm{b}}} \\ &\quad \times \sin\theta_{\tilde{\mathrm{t}}} - 2m_b (\mu + A_b \tan\beta) \sin\theta_{\tilde{\mathrm{b}}} \cos\theta_{\tilde{\mathrm{t}}} \\ &\quad -2m_t (\mu + A_t \cot\beta) \cos\theta_{\tilde{\mathrm{b}}} \sin\theta_{\tilde{\mathrm{t}}} \Big] \end{aligned} \tag{50}$$

$$\begin{aligned} &g[H^+ \text{ out}, \tilde{\mathrm{t}}_1 \text{ in}, \tilde{\mathrm{b}}_2 \text{ out}] = g[H^- \text{ out}, \tilde{\mathrm{t}}_1 \text{ out}, \tilde{\mathrm{b}}_2 \text{ in}] \\ &= \frac{g_2}{2\sqrt{2} m_W} \Big[ \sin 2\beta \Big( m_b^2 (1 + \tan^2\beta) + m_t^2 (1 + \cot^2\beta) \\ &\quad -2m_W^2 \Big) \sin\theta_{\tilde{\mathrm{b}}} \cos\theta_{\tilde{\mathrm{t}}} - 2m_t m_b (\tan\beta + \cot\beta) \cos\theta_{\tilde{\mathrm{b}}} \\ &\quad \times \sin\theta_{\tilde{\mathrm{t}}} + 2m_b (\mu + A_b \tan\beta) \cos\theta_{\tilde{\mathrm{b}}} \cos\theta_{\tilde{\mathrm{t}}} \\ &\quad -2m_t (\mu + A_t \cot\beta) \sin\theta_{\tilde{\mathrm{b}}} \sin\theta_{\tilde{\mathrm{t}}} \Big] \end{aligned} \tag{51}$$

$$\begin{aligned} &g[H^+ \text{ out}, \tilde{\mathrm{t}}_2 \text{ in}, \tilde{\mathrm{b}}_1 \text{ out}] = g[H^- \text{ out}, \tilde{\mathrm{t}}_2 \text{ out}, \tilde{\mathrm{b}}_1 \text{ in}] \\ &= \frac{g_2}{2\sqrt{2} m_W} \Big[ \sin 2\beta \Big( m_b^2 (1 + \tan^2\beta) + m_t^2 (1 + \cot^2\beta) \\ &\quad -2m_W^2 \Big) \cos\theta_{\tilde{\mathrm{b}}} \sin\theta_{\tilde{\mathrm{t}}} - 2m_t m_b (\tan\beta + \cot\beta) \sin\theta_{\tilde{\mathrm{b}}} \\ &\quad \times \cos\theta_{\tilde{\mathrm{t}}} + 2m_b (\mu + A_b \tan\beta) \sin\theta_{\tilde{\mathrm{b}}} \sin\theta_{\tilde{\mathrm{t}}} \\ &\quad +2m_t (\mu + A_t \cot\beta) \cos\theta_{\tilde{\mathrm{b}}} \cos\theta_{\tilde{\mathrm{t}}} \Big] \end{aligned} \tag{52}$$

$$
\begin{aligned}
&g[H^+\ \text{out}, \tilde{\mathrm{t}}_2\ \text{in}, \tilde{\mathrm{b}}_2\ \text{out}] = g[H^-\ \text{out}, \tilde{\mathrm{t}}_2\ \text{out}, \tilde{\mathrm{b}}_2\ \textit{in}] \\
&= \frac{g_2}{2\sqrt{2}m_W}\Big[\sin 2\beta\Big(m_b^2(1+\tan^2\beta)+m_t^2(1+\cot^2\beta) \\
&\quad -2m_W^2\Big)\ \sin\theta_{\tilde{\mathrm{b}}}\sin\theta_{\tilde{\mathrm{t}}}+2m_tm_b(\tan\beta+\cot\beta)\ \cos\theta_{\tilde{\mathrm{b}}} \\
&\quad \times\cos\theta_{\tilde{\mathrm{t}}}+2m_b(\mu+A_b\tan\beta)\ \cos\theta_{\tilde{\mathrm{b}}}\sin\theta_{\tilde{\mathrm{t}}} \\
&\quad +2m_t(\mu+A_t\cot\beta)\ \sin\theta_{\tilde{\mathrm{b}}}\cos\theta_{\tilde{\mathrm{t}}}\Big] \qquad (53)
\end{aligned}
$$

$$
\begin{aligned}
&g[\tilde{\mathrm{t}}_1,\tilde{\mathrm{t}}_1,H^+,H^-] \\
&= \frac{g_2^2}{2}\left[\frac{1}{3}t_w^2\cos 2\beta-\frac{m_t^2}{m_W^2}\cot^2\beta-\cos^2\theta_{\tilde{\mathrm{t}}}\left(\left(\frac{1}{2}+\frac{5}{6}t_w^2\right)\right.\right. \\
&\quad \left.\left.\times\cos 2\beta+\frac{m_b^2\tan^2\beta-m_t^2\cot^2\beta}{m_W^2}\right)\right] \qquad (54)
\end{aligned}
$$

$$
\begin{aligned}
&g[\tilde{\mathrm{t}}_2,\tilde{\mathrm{t}}_2,H^+,H^-] \\
&= \frac{g_2^2}{2}\left[-\left(\frac{1}{2}+\frac{1}{6}t_w^2\right)\cos 2\beta-\frac{m_b^2}{m_W^2}\tan^2\beta+\cos^2\theta_{\tilde{\mathrm{t}}}\right. \\
&\quad \left.\times\left(\left(\frac{1}{2}+\frac{5}{6}t_w^2\right)\cos 2\beta+\frac{m_b^2\tan^2\beta-m_t^2\cot^2\beta}{m_W^2}\right)\right] \qquad (55)
\end{aligned}
$$

$$
\begin{aligned}
&g[\tilde{\mathrm{b}}_1,\tilde{\mathrm{b}}_1,H^+,H^-] \\
&= \frac{g_2^2}{2}\left[-\frac{1}{3}t_w^2\cos 2\beta-\frac{m_b^2}{m_W^2}\tan^2\beta+\cos^2\theta_{\tilde{\mathrm{b}}}\left(\left(\frac{1}{2}+\frac{1}{6}t_w^2\right)\right.\right. \\
&\quad \left.\left.\times\cos 2\beta+\frac{m_b^2\tan^2\beta-m_t^2\cot^2\beta}{m_W^2}\right)\right] \qquad (56)
\end{aligned}
$$

$$
\begin{aligned}
&g[\tilde{\mathrm{b}}_2,\tilde{\mathrm{b}}_2,H^+,H^-] \\
&= \frac{g_2^2}{2}\left[\left(\frac{1}{2}-\frac{1}{6}t_w^2\right)\cos 2\beta-\frac{m_t^2}{m_W^2}\cot^2\beta\right. \\
&\quad \times-\cos^2\theta_{\tilde{\mathrm{b}}}\left(\left(\frac{1}{2}+\frac{1}{6}t_w^2\right)\cos 2\beta\right. \\
&\quad \left.\left.\left.+\frac{m_b^2\tan^2\beta-m_t^2\cot^2\beta}{m_W^2}\right)\right] \qquad (57)
\end{aligned}
$$

## D Feynman graphs

Feynman Graphs with opposite direction of charge flow are not depicted but indicated by dots.

### D.1 Squark-Graphs

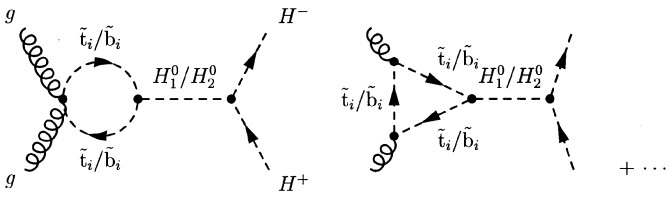


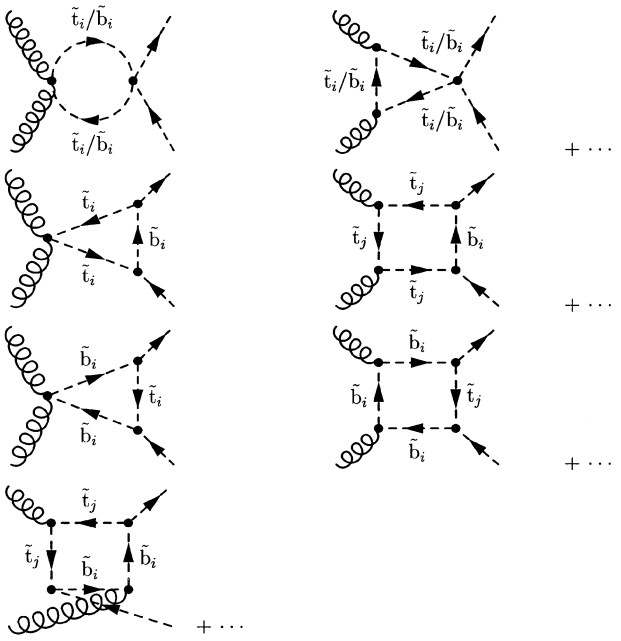


### D.2 Quark graphs

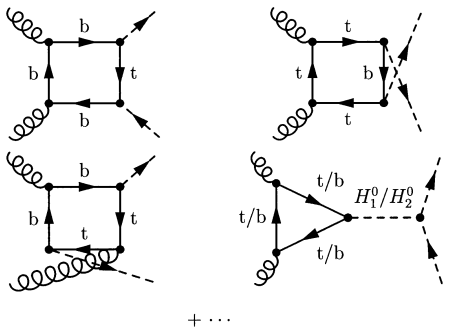


## References


1. E. Eichten, I. Hinchliffe, K. Lane, C. Quigg, *Rev. Mod. Phys.* **56** (1984) 579; N.G. Deshpande, X. Tata, D.A. Dicus, *Phys. Rev.* **D29** (1984) 1527.
2. S.S.D. Willenbrock, *Phys. Rev.* **D35** (1987) 173.
3. A. Krause, T. Plehn, M. Spira, P.M. Zerwas, *Nucl. Phys.* **B519** (1998) 85.
4. A.A. Barrientos Bendezú, B.A. Kniehl, hep-ph/9908385
5. J. Ellis, G. Ridolfi, F. Zwirner, *Phys. Lett.* **B262** (1991) 477; A. Dabelstein, *Nucl. Phys.* **B456** (1995) 25.
6. M.A. Diaz, H.E. Haber, *Phys. Rev.* **D45** (1992) 4246
7. J.F. Gunion, H.E. Haber, G. Kane, S. Dawson, *The Higgs Hunter's Guide* , Addison-Wesley Publishing Company, 1990.
8. E.W.N. Glover, J.J. van der Bij, *Nucl. Phys.* **B309** (1988) 282.
9. T. Plehn, M. Spira, P.M. Zerwas, *Nucl. Phys.* **B479** (1996) 46
10. G. Sterman et al, *Rev. Mod. Phys.* **67** (1995) 1.
11. A.D. Martin, W.J. Stirling, R.G. Roberts, *Phys. Lett.* **B354** (1995) 155.